Electric Field Effects in Flash Joule Heating Synthesis

Lucas Eddy,[1,2#] Shichen Xu,[2#] Changhao Liu,[3] Phelecia Scotland,[4] Weiyin Chen,[2] Jacob L. Beckham,[2] Barbara Damasceno,[2] Chi Hun Choi,[4] Karla Silva,[2] Alexander Lathem,[1,2] Yimo Han,[4] Xinfang Zhang,[3]* Yufeng Zhao,[4,5]* and James M. Tour[2,4,6,7]*

[1]*Applied Physics Graduate Program and Smalley-Curl Institute,* [2]*Department of Chemistry,* [3]*School of Metallurgical and Ecological Engineering, University of Science and Technology Beijing, Beijing, 100083 P. R. China,* [4]*Department of Materials Science and NanoEngineering,* [5]*Department of Physics, Corban University, 5000 Deer Park Drive SE, Salem, OR 97317, United States* [6]*Smalley-Curl Institute, the NanoCarbon Center, and the Rice Advanced Materials Institute, and* [7]*Department of Computer Science, Rice University, 6100 Main Street, Houston, Texas 77005, United States*

*Corresponding Authors (Emails: xfzhang@alum.imr.ac.cn, yzhao@corban.edu, tour@rice.edu)

#These authors contributed equally to this work.

Abstract Flash Joule heating has emerged as an ultrafast, scalable, and versatile synthesis method for nanomaterials such as graphene. Here, we experimentally and theoretically deconvolute the contributions of thermal and electrical processes to the synthesis of graphene by flash Joule heating. While traditional methods of graphene synthesis involve purely chemical or thermal driving forces, our results show that the presence of charge and the resulting electric field in a graphene precursor catalyzes the formation of graphene. Furthermore, modulation of the current or the pulse width affords the ability to control the three-step phase transition of the material from amorphous carbon to turbostratic graphene, and finally to ordered (AB and ABC-stacked) graphene and graphite. Finally, density functional theory simulations reveal that the presence of

charge- and current-induced electric field inside the graphene precursor facilitates phase transition by lowering the activation energy of the reaction. These results demonstrate that the passage of electrical current through a solid sample can directly drive nanocrystal nucleation in flash Joule heating, an insight that may inform future Joule heating or other electrical synthesis strategies.

Keywords: flash graphene, phase transition, flash Joule heating, electric field, molecular dynamics

Introduction

The application of electric fields in materials synthesis has emerged as a prominent and captivating research area in modern science and engineering.[1-3] An external electric field is widely used to tune the activation energy of chemical products,[4] allowing thermochemical reactions to occur at lower temperatures,[5] and to tune the crystallite size[6] and alignment[7] of inorganic products. The electric field strength used in these techniques is typically on the order of 10^4 to 10^9 V/m, though fields as low as 10^2 V/m have been demonstrated to affect the reaction product.[8] An external electric field can change the synthesis products, and it has also been suggested that the presence of an electric field can have an effect on the motion of electrically neutral particles.[9]

Flash Joule heating (FJH), as a method exhibiting high energy efficiency and an ultrafast heating rate, has recently been used in the synthesis of many materials including graphene,[10-16] transition metal chalcogenides,[17] and various other carbide and inorganic compounds.[18-21] It has also been widely explored as a method for effective remediation of soil[22] and battery electrodes[23] as well as a method for recycling and upscaling materials.[24-26] In contrast to conventional chemical heating methods, which use conductive or radiative heating, Joule heating requires an electric current to

flow through the sample itself, which in turn directly heats the feedstock. Passing this electric current through the reactants involves imposing an electrical potential difference, typically up to several hundred volts, across a reaction vessel that is several centimeters across, leading to average electric fields on the order of 10^3-10^4 V/m, and a current density of 10^5-10^7 A/m^2. In the synthesis of flash graphene (FG), our previous studies have found that thermal annealing alone could not account for the formation of highly turbostratic particles,[11] suggesting a direct role for the passage of current through the material in the nucleation of graphene crystals. Now that the synthesis of FG has been scaled up,[15] a deeper understanding of the FG growth process is necessary to enable more precise control over the structure and quality, namely crystallinity, defect density, and turbostratic character, of FG for various applications.

Here, we experimentally deconvolute the electrical and thermal effects of FJH in the conversion of metallurgical coke to graphene to examine the input that each one has on the reaction enthalpy, activation energy, and product distribution. The enthalpy changes occurring during the FG synthesis using both electrothermal and purely thermal flash reactions demonstrate that the electric field strength affects the morphology of the carbon feedstock as it is converted from amorphous carbon (AC) to turbostratic (inter-sheet misalignment) FG and finally to ordered FG and graphite, which is composed of both Bernal (AB) and rhombohedral (ABC) stacked layers.[27] In addition, both experimental and theoretical studies demonstrate that oscillating the current density of the reaction through pulse width modulation facilitates this phase transition. Finally, theoretical simulations demonstrate that an induced electric field inside the graphene precursor drives the phase transition by lowering the activation energy of the reaction. These results show that chemical

reactions can be driven directly by the flow of current in flash Joule heating reactions, deepening our understanding of the mechanisms driving nanocrystal formation in this process.

Results and Discussion

Essential to the deconvolution of the electrical and thermal effects of FJH is a reaction vessel architecture that permits the heat of a flash reaction to pass through the sample while blocking current. First, we developed such a reaction vessel (**Figure 1a)**. During a flash reaction in this vessel, the electrical current will pass primarily through the carbon paper platform, which is more conductive than the metallurgical coke resting above and in contact with the electrodes at both ends of the vessel, minimizing the current through the metallurgical coke is minimal. In this way, the metallurgical coke is heated through thermal conduction by its contact with the underlying carbon paper. By contrast, the reaction tube architecture used in conventional flashing **(Figure 1b)** passes the electrical current through the metallurgical coke itself, which is in full contact with the electrodes. These two distinct methods were performed with samples with the same mass, resistance, and flashing energy, resulting in similar flashing temperature profiles **(Figures 1c-d)**. Despite keeping all these factors constant, the products produced by these two reaction schemes are dramatically different.

Raman spectroscopy is a commonly used technique for the identification and characterization of graphene. Raman spectra of graphene and graphite contain the second-order overtone of the D band, referred to as the 2D band. The appearance of this band is a positive indicator for the formation of a graphitic lattice, and its shape and intensity offer important nanostructural information.[27-28] Spectra of high-quality FG contain a resonance-enhanced single-Lorentzian 2D

band with a narrow full width at half maximum (FWHM; ~16 cm^{-1}) and a magnified I_{2D}/I_G peak intensity ratio (up to a maximum of 17) as compared to pristine single-layer graphene (which possesses I_{2D}/I_G of ~3). Statistics on individual spectra illustrate relationships between the I_{2D}/I_G ratio, the FWHM of the 2D band, and the position of the 2D band, showing a blue-shifted and narrowed 2D band at high I_{2D}/I_G which is indicative of resonance-enhanced turbostratic graphene.[10,29] In a Raman spectrum, graphene exhibits a G peak, which is common among ordered carbon materials, a D peak, which is correlated with the defect density, and a 2D peak, which changes in shape and intensity in accordance with crystallinity and layer-stacking. Consequently, we evaluate graphene conversion and quality (crystallinity, defect density, and turbostratic character) by considering the ratio of the intensity of the D peak that of the G peak (referred to as $I_{D/G}$) as a metric for defect density and the ratio of the intensity 2D peak to that of the G peak ($I_{2D/G}$) as a metric for graphene conversion. Even though a higher voltage, and consequently more energy, was used in the purely thermal flash reaction, the graphene quality is significantly better in the electrothermal flash architecture, exhibiting a low $I_{D/G}$ and a high $I_{2D/G}$ **(Figures 1e-f)**.

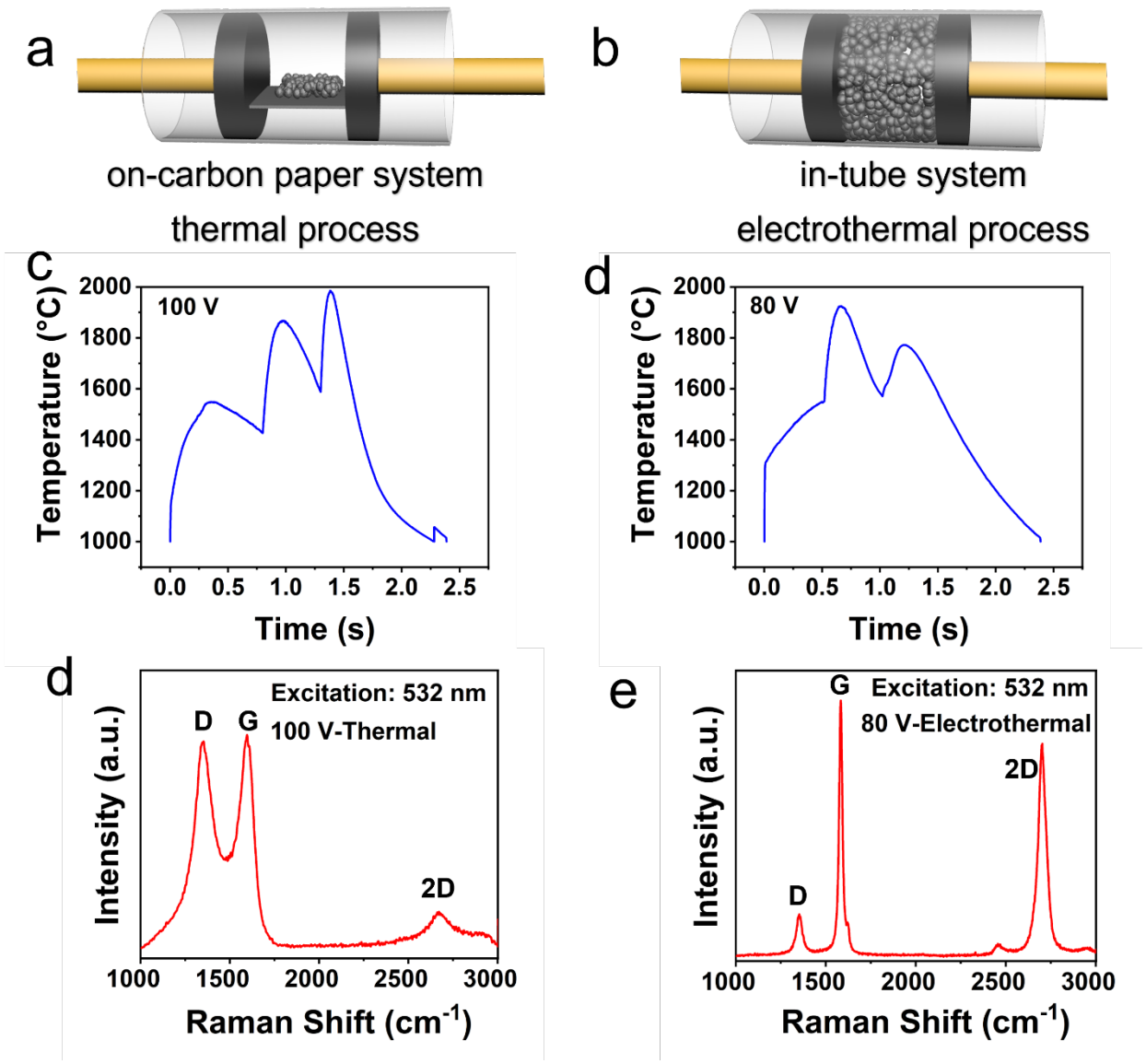

Figure 1. Comparison between thermal and electrothermal systems. a) Schematic illustration of the carbon-paper based "2D" flashing system used to perform thermal flashes. By this scheme, most electric current passes under rather than through the carbon feedstock. Thus, the reaction mechanism is predominantly by thermal conduction. b) Schematic illustration of the standard, tube-based flashing system used to perform electrothermal flashes. By this scheme, electric current passes through the metallurgical coke amorphous carbon (MCAC) feedstock itself, exposing it to an electric field and heating by resistive Joule heating between the granules of MCAC that are

0.30-0.84 mm in size. c) Temperature profile of a thermal flash performed at 100 V. d) Temperature profile of an electrothermal flash performed at 80 V. The temperature profiles of both reactions are comparable in both the max temperature achieved and the duration of the reaction. A feedstock of 120 mg of MCAC was used for both reactions. d) Representative Raman spectrum of the product of a thermal flash performed at 100 V. There is little graphene character noted by the small and broad 2D peak. e) Representative Raman spectrum of the product of an electrothermal flash performed at 80 V. The product of this flash is predominantly flash graphene, as demonstrated by the sharp and high 2D peak, despite being reacted with less energy than in the thermal 100 V reaction. Additional Raman spectra and temperature profile comparisons are illustrated in **Figures S1-S3.**

The experimental results suggest that the passage of electric current itself through the MCAC sample reduces the energy requirement for graphene conversion. This finding is consistent with previous observations of flash graphene morphologies, in which two distinct morphologies were found to form in FJH reactions using a carbon black precursor.[11] The "wrinkled" morphology was found to form under simple thermal annealing and exhibited a Raman spectrum similar to the thermal-only flash shown in **Figure 1d**. The turbostratic FG morphology exhibited large, turbostratic flakes and showed a Raman spectrum similar to that shown in **Figure 1e.** Thermal annealing alone was previously found to be insufficient to nucleate large turbostratic FG flakes.

To examine this energy difference more precisely, we performed several panels of reactions under both the thermal and electrothermal reaction architectures and compared graphene quality of the products using Raman spectroscopy analysis. For each graphene product, Raman spectroscopy

measurements were performed twice on each of 100 points, evenly spaced in a square grid across a 1 mm^2 area of the sample. From these 200 total scans, the average $I_{2D/G}$ and $I_{D/G}$ ratios were calculated. Among the measurements with a discernible G peak, the portion of those with a $I_{2D/G}$ ratio of at least 0.3 were counted as a portion of the total of samples with a discernible G peak. This portion is equal to the graphene yield per an established protocol.[16]

When the flash reaction is performed with MCAC under both architectures at the same voltage and mass, and thus at the same energy density **(Figure 2a)**, the $I_{2D/G}$ peak ratio is higher and the $I_{D/G}$ peak ratio is lower in the electrothermal case. Furthermore, at this energy density of 6 kJ/g, the graphene yield is 98% in the electrothermal case but only 5% in the thermal case. Hence, merely changing the flashing architecture has a dramatic effect on the graphene quality at a given energy. A panel of flashes were performed at different energies under both experimental architectures until the graphene quality and conversion of a reaction with electrothermal architecture was comparable to the graphene quality and conversion of a reaction with thermal architecture **(Figure 2b)**. Additional reactions from this panel are shown in **Figure S4**. Even though ~4.5x more energy (19 kJ/g) is used in the thermal architecture here, the graphene quality of the electrothermal flash is superior. This is consistent with the idea that the passage of electrical current is necessary to drive the formation of large, turbostratic graphene flakes, which exhibit resonance-enhanced I_{2D} in the Raman spectrum.[11] To explore this effect further, additional flash reactions were performed at constant energy and mass, but at different flash voltages and therefore different electric field strengths **(Figure 2c)**. These results indicate that graphene conversion and quality are proportional to the strength of the electric field applied, while independent of the energy of the reaction.

In theory, after conversion from MCAC to turbostratic graphene by flash Joule heating, sufficient energy can further convert turbostratic graphene into ordered graphene and graphite. Using a merely thermal reaction architecture, the activation energy of the MCAC to turbostratic FG was measured to be 410 kJ/mol (34 kJ/g) **(Figure 2d)**. Electrothermal flashing results at the same scale are more efficient than thermal flashing results (**Figure 2e)**. The energy required to achieve conversion to ordered graphene by electrothermal flash Joule heating at the same scale has been measured here as ~2x that required to achieve conversion to turbostratic graphene. DFT calculations of thermal flash Joule heating-induced transition similarly predict that ~2.5x more energy is required to convert turbostratic graphene to ordered graphene as is required to transition from amorphous carbon to turbostratic graphene (**Figure 2f)**. Furthermore, these calculations reveal these two transitions to be exothermic, suggesting that the release of chemical energy also assists the carbon feedstock in achieving the ~3000 °C afforded during the conversion of MCAC to high-yield FG. Larger-scale reactions suffer less heat loss to the environment per gram of graphene produced. Consequently, at 5.7 g scale, the activation energy of the MCAC to turbostratic FG transition is only 90 kJ/mol (7.5 kJ/g) as previously reported **(Figure 2g)**.[15] This value is ~2.6x less than that calculated for the same transition with a purely thermal reaction with 100% thermal efficiency.

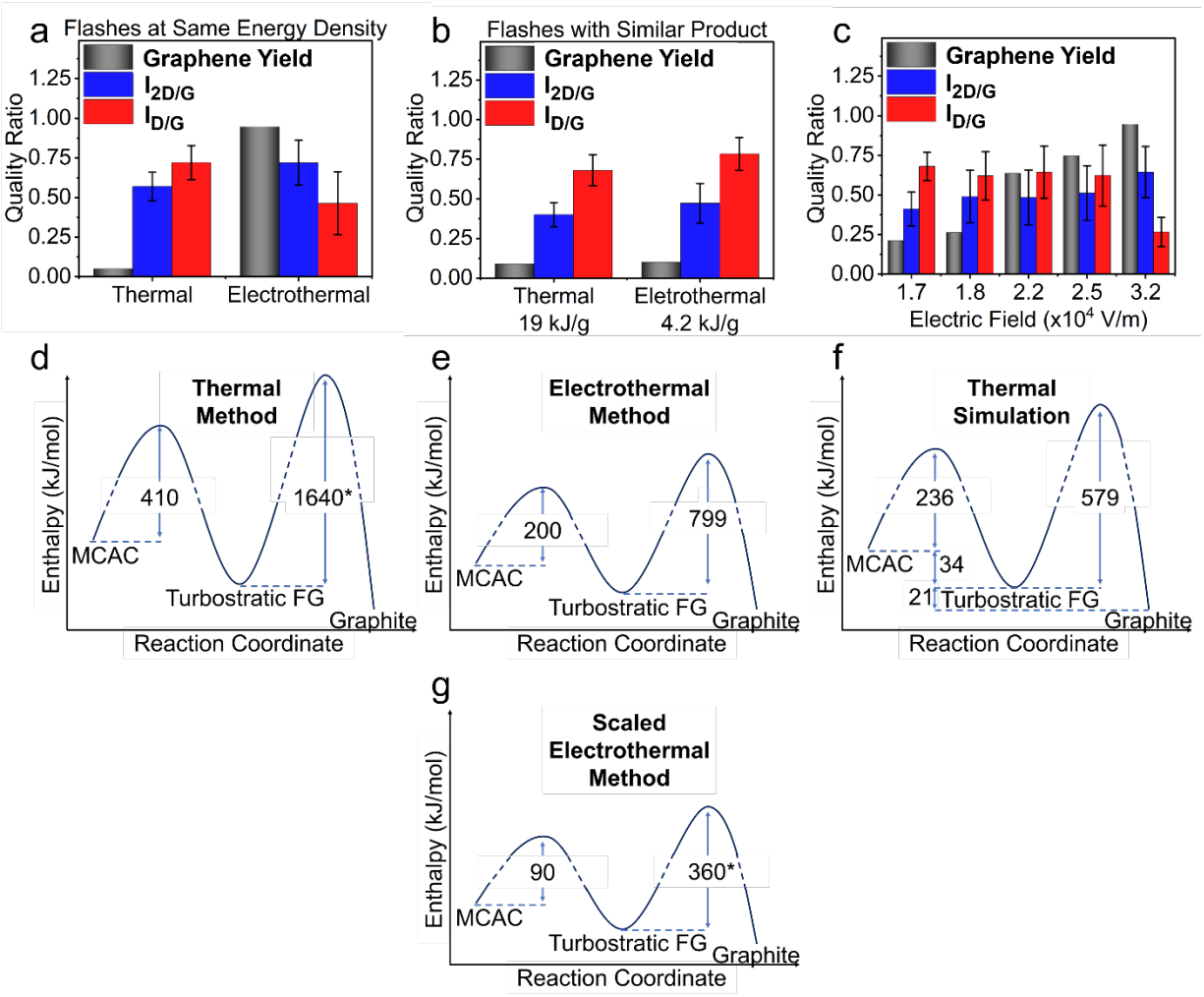

Figure 2. Effect of electric field on the flash reaction and products. a) Graphene quality comparison of MCAC flashed in 120 mg batches at the same energy density (energy/mass) but using different flash architectures evaluated by Raman spectroscopy analysis. b) Graphene conversion and quality comparison of MCAC of comparable product quality at different flashing energy densities. The graphene yield of the product in the thermal case is 9%, while the graphene yield of the product in the electrothermal case is 10%, which demonstrates the near-minimum energy requirement at which conversion begins. Additional Raman spectra of electrothermal flashes at different energies are shown in **Figure S5-S6**. c) Graphene quality of MCAC flashed electrothermally at different electric fields but at a constant energy density. Higher electric fields

were achieved by increasing the voltage of the flash and reducing the capacitance such that the energy of each flash remained constant. The electric field strength was determined by dividing the voltage of the flash by the length of the resistive sample through which current flows. The graphene quality and conversion are improved by the presence of a stronger electric field, even at constant energy. The average Raman spectra of these scans are shown in **Figure S7**. d) Reaction progress diagram of activation energies by the thermal method at a 120 mg scale. *The activation energy from turbostratic FG to graphite is estimated from the electrothermal data because we could not input enough energy to effect the thermal transition to graphite. Specifically, comparing the first-step measured energies of 799/200 = 4.00 and using the same ratio of difference: 410 x 4.00 = 1640. e) Reaction progress diagram of enthalpy by the electrothermal method. These results were obtained from flashing with 120 mg batch size. The activation energy to obtain turbostratic FG from MCAC was measured to be 200 kJ/mol (16.7 kJ/g), while the activation energy to obtain graphite from turbostratic FG was measured to be 799 kJ/mol (66.5 kJ/g). f) Density-functional theory (DFT)-determined reaction progress diagram displaying simulated enthalpies of the transition reactants and products by a thermal heating scheme. g) Reaction enthalpy of a previously reported scaled (5.7 g) reaction.[15] At this scale, the transition from MCAC to turbostratic FG is achieved at an activation energy of 90 kJ/mol (7.5 kJ/g). The activation energy value for the turbostratic FG to graphite transition is extrapolated in the same manner as in the thermal case.

The transition from MCAC to turbostratic graphene and finally to ordered graphene and graphite is accompanied by microscopic and spectroscopic changes in the carbon product. These changes can be observed by flashing the MCAC at different voltages to stop the reaction at different points in the transition **(Figure 3)**. At sufficiently low voltage and therefore energy, MCAC remains

unconverted and thus does not exhibit any ordered structure under TEM **(Figures 3a, S8a)**. As the flashing voltage increases, ordered structure begins to emerge in the product along with the alignment pattern indicative of turbostratic graphene **(Figures 3b-c and S8b-c)**. At high voltages, ordered graphitic sheets are observed under TEM. When these sheets accumulate to be 10 or more layers thick in a region, then the region is determined to be graphite rather than merely ordered graphene **(Figures 3d, S8d)**.[28] While nanoscale characterization methods can verify the existence of graphene in a sample, bulk characterization methods are essential to evaluate graphene conversion over a large sample. Raman spectroscopy likewise illustrates that as a function of the flashing voltage, the $I_{2D/G}$ peak ratio increases, and the $I_{D/G}$ peak ratio decreases **(Figures 3e, S9)**. As MCAC is converted to turbostratic FG, turbostratic-indicative TS_1 and TS_2 peaks begin to emerge **(Figure S10a)**. As the turbostratic FG is converted to ordered FG, these TS peaks vanish, and a Bernal-indicative M peak emerges **(Figure S10b)**. X-ray diffractometry illustrates that the (002) graphene peak, corresponding to the lattice plane that is oriented perpendicular to the graphene sheets, sharpens and shifts to a higher angle as the carbon layers stack and decrease in spacing **(Figures 3f)**. As the turbostratic graphene layers align to AB- or ABC-stacked orientations, the interlayer spacing consequently decreases **(Figure 3g, S11)**. Turbostratic MC-derived FG typically exhibits an interlayer spacing of ~0.341 nm, while ordered graphene exhibits spacing of 0.338 nm. The disordered-ordered graphene ratio in the sample is linearly proportional to the graphene interlayer spacing **(Figure S12)**. This interlayer spacing changes as well as the emergence of a more prominent 2H (101) peak **(Figure S13),** providing more evidence of this transition in the bulk sample.

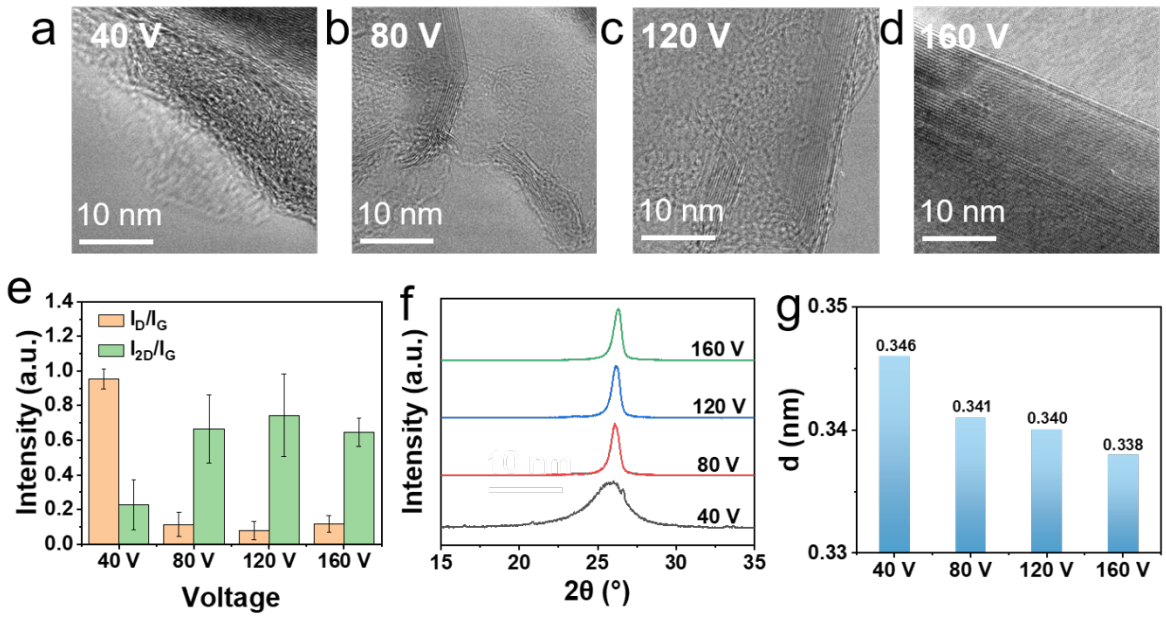

Figure 3. Carbon phase transition process at different voltages. a) TEM images of the products of 120 mg batches of MCAC flashed at 40 V, b) 80 V, c) 120 V, and d) 160 V. As the MCAC feedstock is flashed at higher voltages, the products transition from an amorphous carbon structure to a turbostratic flash graphene structure to finally a graphite structure. e) Graphene quality of the products of these flashes as determined by Raman spectroscopy analysis. Flashing at higher voltages improves graphene crystallinity and reduces defect density (increases the $I_{2D/G}$ and decreases the $I_{D/G}$ peak ratios). Only points exhibiting a $I_{2D/G}$ ratio above 0.3 are assigned to be graphene. f) XRD patterns highlighting the 002 peak at ~26°, which indicates the interlayer spacing of the carbon lattices. Higher voltages result in both a sharpening of this peak and a slight shift to higher angles, corresponding to increased crystallinity and reduced interlayer spacing. g) Illustration of the average interlayer spacing in nm above each bar of the flash products as determined from the (002) XRD peak.

As discussed previously, flash graphene quality and conversion are a function of the voltage, capacitance, energy, mass and tube size.[15-16] We also found that additional flashes, even at the same energy, can further improve graphene quality over that produced by the initial flash **(Figure S14)**. The improvement in FG quality upon reflashing is proportional to the energy used **(Figure S15)**. FG flashed at higher voltages and thus with different interlayer spacing has measurably different surface area and dispersibility in solution **(Figure S16)**; hence, the ability to control the graphene characteristics is important.

Pulse-width modulation (PWM) has been previously demonstrated to improve both graphene yield and uniformity when oscillated at a 1 kHz frequency.[15] Thus, the implementation of oscillating the current by PWM, which in turn oscillates the carbon heating profile, enables flash graphene to be produced at a lower energy cost. To investigate this further, DFT calculations were performed on the thermal heating synthesis of turbostratic graphene from AC **(Figures 4, S17, S18)**, in one simulation while maintaining a constant temperature profile **(Figure 4a-b)** and in another while varying the temperature at a constant frequency **(Figure 4c-d)**. The simulation of the constant temperature profile heating case demonstrates no phase transition from amorphous carbon to graphene. However, when the temperature is allowed to oscillate, even at the same average heating rate, a transition from amorphous carbon to turbostratic graphene is observed. Furthermore, the rate at which this transition occurs is proportional to both the frequency and the amplitude of the temperature oscillation. The effect that PWM has on graphene conversion is further demonstrated through experimental results. By introducing PWM duty cycles, an oscillating current profile can be obtained **(Figure 4e)**. Despite being flashed at the same energy, FG synthesized by oscillating the current at 1 kHz with PWM exhibits slightly improved graphene quality (higher crystallinity

and lower defect density) and significantly improved graphene uniformity compared to FG synthesized by unmodulated DC current **(Figure 4f)**. Additional results of experiments examining the effects of PWM of the graphene products are also illustrated in **Figure S18-S21**. Though PWM improves graphene quality, small changes in the PWM frequency do not have a significant effect on graphene quality **(Figure S22)**. When reflashes are performed with more intense duty cycles, the graphene quality is relatively unaffected, but the interlayer spacing decreases more significantly than seen with less intense duty cycles **(Figure S23)**.

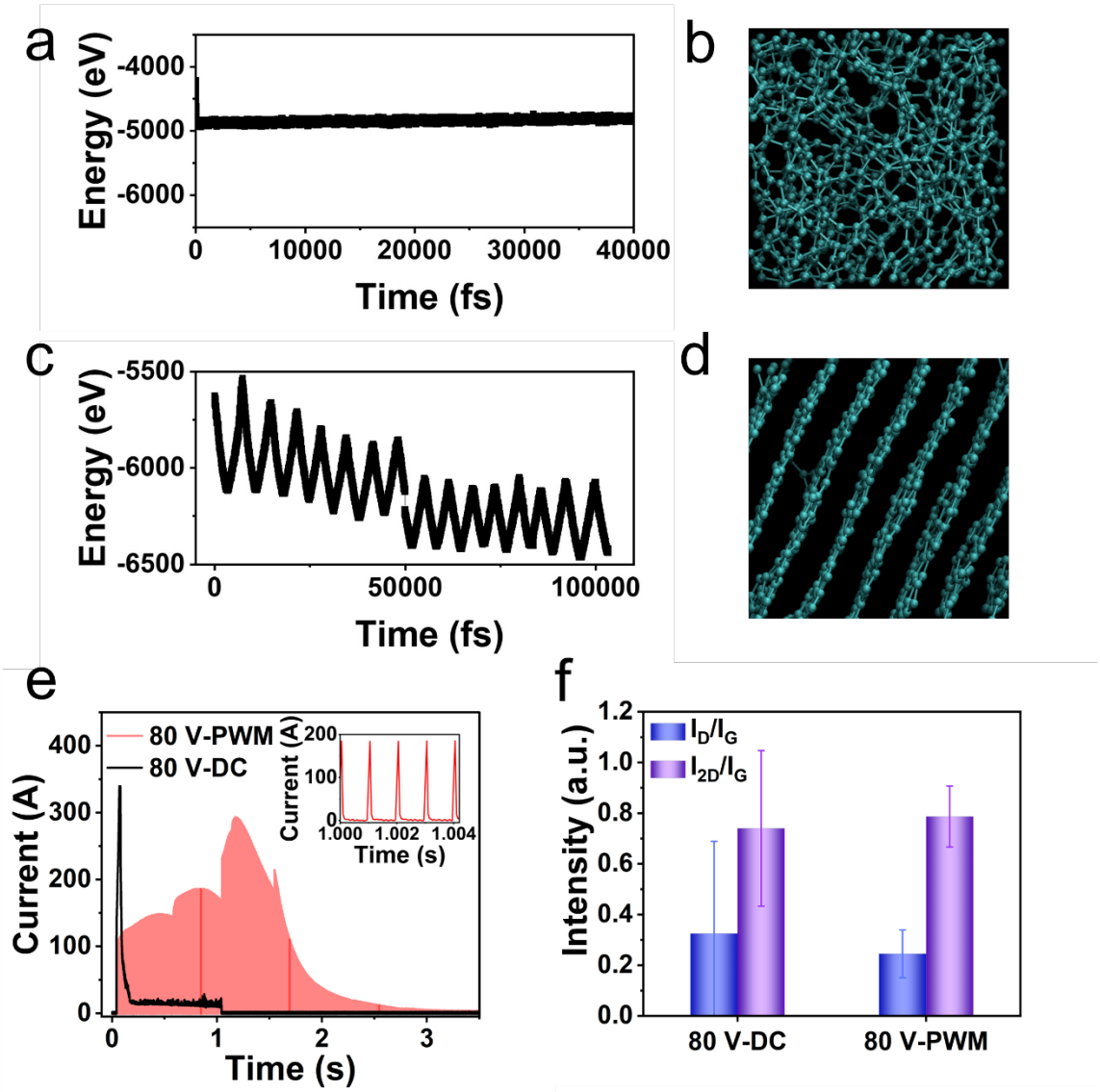

Figure 4. The effect of temperature oscillation on the graphene phase transition a) Simulated energy of the structure while heating at a constant temperature. The structure prior to heating is shown in **Figure S18a**. b) Simulation illustration of AC after being heated for 40 ps at 3200 K. Some initial ordering is visible in the structure. c) Simulated energy of the structure while heating at a variable temperature over 100 ps. d) Simulation illustration of the resulting turbostratic graphene lattice after 100 ps at a variable temperature oscillating between 1000-4000 K at a rate of 1 K/fs. e) Experimental current profiles of flashes on MCAC performed by PWM (red) and flashes performed via a direct current (DC) discharge (black). Both flashes discharged the same amount of energy into the sample, but the current oscillates by PWM at a frequency of 1 kHz. This results in a 1 kHz level oscillation in the heating of the sample. The inset illustrates the PWM duty cycles in closer detail. f) Illustration of graphene quality of MCFG products determined by Raman spectroscopy analysis.

Additional theoretical calculations were performed to further elucidate the effect that running an electric current through the sample by an applied voltage has on the flash Joule heating reaction **(Figure 5)**. Under the influence of an electric field, the randomly distributed carbon atoms in AC begin to align themselves, ultimately forming aligned graphene layers with a lower electric free energy **(Figure 5a)**. As electric current passes through the carbon atoms, high current density and thus a high localized electric field results on the surface of the carbon atoms **(Figure 5b)**. Thus, even though the average electric field across a flashing vessel is ~10^4 V/m, the electric field localized around these carbon atoms can be far higher. Additionally, the presence of this electric current energetically favors reorientation of the graphene layers along the direction of the electric field **(Figure 5c)** and ordering of the graphitic lattice to reduce the interlayer spacing **(Figure 5d)**.

Both of these effects are proportional to the strength of the applied voltage and therefore to that of the electric field present in the reaction sample.

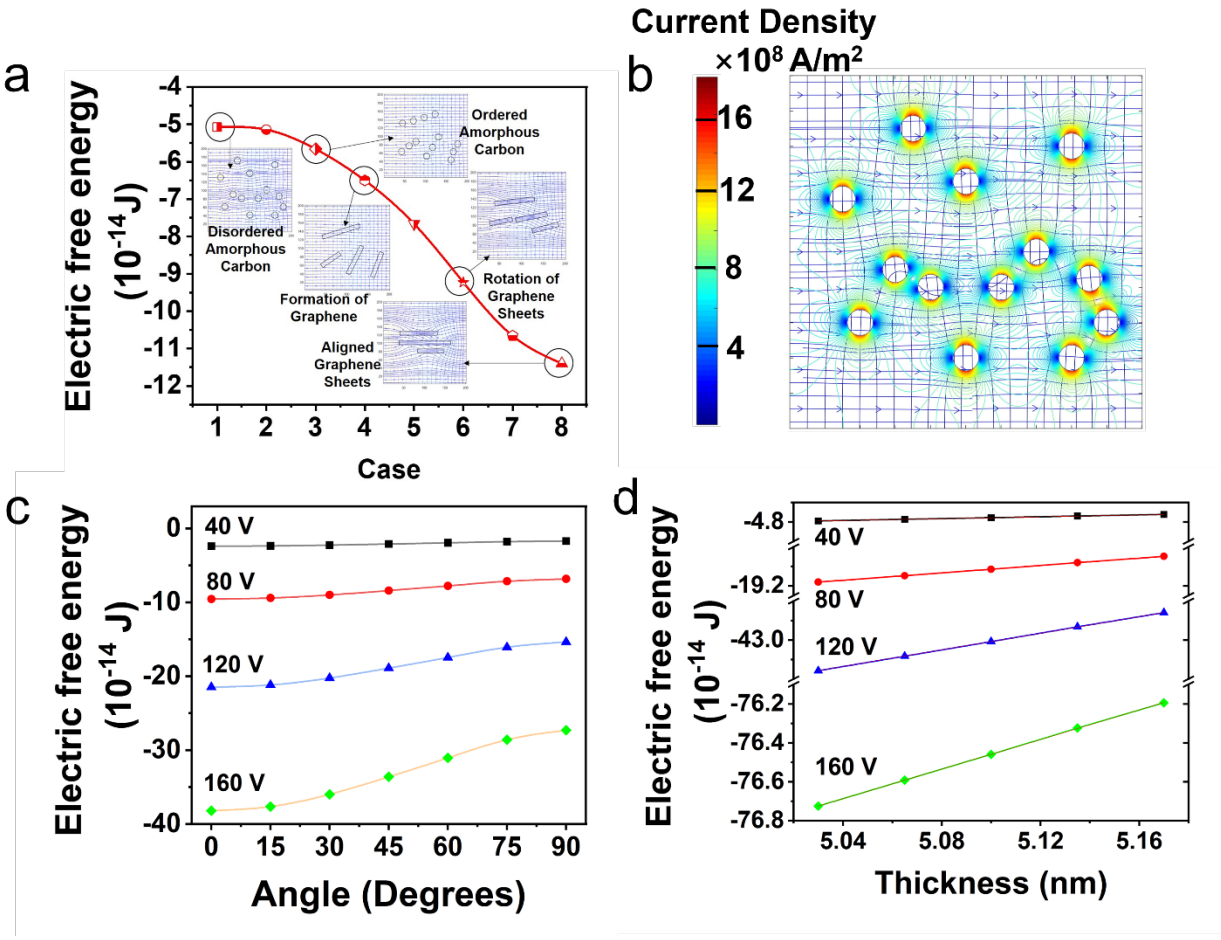

Figure 5. Simulation results of the phase transition. a) Simulation results illustrating the change in electric free energy during graphene sheet alignment. The reaction from AC to FG is exothermic. b) 2D simulation illustration of the charge density distribution across AC flakes when subjected to an electric current. Electric charge accumulates on the AC surface, leading to heightened electric field strength localized around the edges of the flakes. c) Simulation results illustrating the change in electric free energy of graphene sheets when oriented at different angles relative to four different electric current densities. The derivative of this graph is also shown in **Figure S24**. d) Simulation results illustrating the effect of graphene thickness along the *c* crystalline axis on the electric free

energy when the sheets are aligned with respect to an electric current. The thickness of the graphene lattice is proportional to the free energy reduction induced by the electric current. This graph is also shown in more detail in **Figure S25.**

Conclusion

We have demonstrated through both experiment and theoretical simulation that the conversion of AC to FG by flash Joule heating is an electrothermal rather than merely a thermal process, and the conversion process can be further assisted by using PWM to oscillate the current. When the electric current passes through the reactant itself, it can greatly facilitate the phase transition process. By changing the flash voltage, the phase control from AC to turbostratic graphene then to graphite can also be realized. Both experimental data and DFT calculations show the energy requirements in the electrothermal process is ~2x lower than in the thermal process. The energy for conversion from turbostratic graphene to graphite is ~4x higher than conversion from AC to turbostratic graphene. Finally, finite difference method was used to analyze and explain the significant roles of current and electric field in the phase transition process.

Materials and Methods

Materials

Metallurgical coke was obtained from SunCoke in chunks ~10 cm in diameter. These chunks were then ground to a diameter of 0.30-0.84 mm. Additional characterization of this raw material has been previously reported.[15]

Flash Joule Heating

Flash Joule heating reactions were performed using two separate flash Joule heating systems. The reactions done at variable electric fields presented in **Figure 2c** were performed using an unmodulated DC system with additional capacitor banks that were connected to the system such that flash reactions could be performed at any 18 mF interval between 59.2 mF and 221.2 mF. All other flash reactions were performed using a 0.624 F capacitor discharge system previously exhibited.[15] Among the reactions performed with this system, only the DC reactions presented in **Figure 4** implemented an unmodulated DC discharge. All other reactions used a 1 kHz pulse-width modulated discharged with a duty cycle sequence, except when explicitly stated, of 10% for 1 s, followed by 20% for 0.5 s, and ending at 50% for 5 s.

All flash Joule heating reactions are operated using a custom LabVIEW program. Current profiles are measured at 50 μs resolution by a Tamura L34S1T2D15 Hall effect sensor, operated by a custom LabVIEW program. Temperature is measured using a Micro-Epsilon CTRM1H1SF100-C3 pyrometer at 1 ms resolution.

Raman Spectroscopy Analysis

Raman spectra were collected using a Renishaw inVia microscope outfitted with a 5 mW, 532 nm laser and a 50x objective lens. Except where explicitly stated, all Raman spectra were collected as follows: 2 Raman spectra were measured on each of 100 points across a square 1 mm^2 grid on the sample using a map scan with LiveTrack focusing software enabled. The average Raman spectra shown for each sample is the average of these 200 spectra. The $I_{2D/G}$ and $I_{D/G}$ ratios and their standard deviations are calculated from these 200 spectra per sample as well using a custom Python program as previously described.[29] Graphene yield is a metric that describes the amount of product that has been converted to graphene as a portion of the total product. For the 200 spectra of each sample, a custom Python program first determines the number of these spectra

that have a discernible G peak. Among these spectra, the program counts the portion of which that has a $I_{2D/G}$ peak ratio of at least 0.3. This portion is equal to the graphene yield. A spectrum without a discernible G peak in a carbon sample most often results from the Raman laser being insufficiently focused.

X-ray Crystallography Analysis

X-ray diffractometry scans were performed using a Rigaku Smartlab II using zero background sample holders, a 40 kV, 30 mA X-Ray source, and a Cu K-β filter.

Transmission Electron Microscopy Analysis

Transmission electron microscopy (TEM) images were collected using FEI Titan Themis operating at 300 keV with the convergence angle of 25 mrad. The aliquot of sample (5 mg of sample/1 mL ethanol) was prepared and was sonicated for 1 h to ensure homogeneous dispersion. The resultant aliquot was drop casted on Cu/lacey carbon TEM grid (Ted Pella). The resultant grid was dried at 80 °C with overnight vacuum drying.

Computational Methods

Density Functional Theory (DFT)

Density Functional Theory (DFT) methods[30] are used as they are implemented in the Vienna Ab-initio Simulation Package (VASP).[30] A plane wave expansion up to 500 eV is employed in combination with an all-electron-like projector augmented wave (PAW) potential.[31] Exchange-correlation is treated within the generalized gradient approximation (GGA) using the functional parameterized by Perdew-Burke-Ernserhof.[32] For all the MD simulation of turbostratic graphitic materials, the supercells are big enough (with 720 C atoms inside the box of size ~ 18.0 Å × 18.0 Å × 18.0 Å), and only the Γ point is used for the Brillouin zone integration over Monkhorst-Pack type mesh.[33] The van der Waals interaction is evaluated within DFT-D3 method

developed by Grimme *et. al*.[34] In structure optimization using the conjugate-gradient algorithm, both the positions of atoms and the unit cells are fully relaxed so that the maximum force on each atom is smaller than 0.01 eV/Å. The MD simulation is performed using Nose-Hoover thermostat and NVT ensemble with a time step of 1 fs. For calibration, we optimized the crystal lattice structure of graphite and the standard lattice constants a = 2.467 Å, c = 6.794 Å were obtained.

For modeling the growth of turbostratic graphene layers, we use randomly generated coordinates of carbon atoms inside a cubic box with the C-C distance no less than 1.5 Å. To mimic the highly nonequilibrium FJH synthesis, a variable temperature MD (VTMD) simulation was used with the temperature fluctuating at the range of 1500 - 4000 K at a rate of 0.2-1.0 K/fs. The VTMD mode of modeling significantly facilitates the crystallization. In contrast, the normal constant temperature MD (CTMD) followed by fast cooling more likely leads to the formation of amorphous carbon with 3D bonding network. Therefore, CTMD was used to model the formation of amorphous carbon and the VTMD to simulate the growth of multilayered turbostratic graphene. All the MD simulation jobs were started from the same initial atomic configuration in which the coordinates of the C atoms were randomly generated. The time scale of simulation is set typically to be 50 ps for the CTMD of AC and 100 ps for the VTMD turbostratic graphene, which were followed by fast cooling down to 100 K at the rate of 0.2 K/fs. Then the structures were optimized to obtain the total energy and material density. Regardless of the structure difference in different situations, the values of energy and material density of amorphous carbon are consistently similar. So are those for the turbostratic graphene. But the AC is distinctively different from the turbostratic graphene.

Phase transition from AC to layered turbostratic graphene were regularly realized in the

VTMD simulations, however, the transition from layered turbostratic graphene to ideal, ordered graphene were never realized within the similar time scale of simulation. This indicates that the activation energy of the latter process is much higher than that of the former. Using the Arrhenius equation, $P = \nu_0 e^{-E_a/kT}$ by setting P = 1/100 ps, T = 2500 K (average), and $\nu_0 = 10^{15}$ Hz, the estimated activation energy for the phase transition from amorphous carbon to turbostratic graphene is E_a= 2.5 eV or 236 kJ/mol. The mechanism of phase transition from turbostratic graphene to ideal graphene is annihilation of the topological defects such as the 5/7/7/5 through Stone-Wales bond flips.[35-36] Therefore, the activation energy of phase transition from turbostratic graphene to ideal graphene is roughly that of the bond flips, ~ 6.0 eV or 579 kJ/mol according to Samsonidze et. al.[37]

Finite Difference Method

To explore the phase transition under the influence of current induced electric field, finite difference method was used to calculate the electrical free energy. The first model was divided into 200 × 200 grids, with each grid having a size of 0.1 × 0.1 nm². Within these grids, circular shapes represented disordered carbon atoms, while rectangle shapes represented graphene sheets formed by the fusion of carbon atoms. This allowed us to calculate the change in electrical free energy as irregular carbon atoms orderly arranged into graphene sheets under the influence of the electric field, followed by the subsequent orderly arrangement of graphene sheets. The electrical potential within this system satisfied Laplace Equation: $\nabla^2\varphi_c = 0$ and $\nabla^2\varphi_g = 0$, where φ_c and φ_g are potentials of carbon atoms and graphene sheet, respectively. To investigate the effect of the electric field, particularly the local electric field, on the transition from amorphous carbon to graphene, we further calculated the current density distribution when the current passes through randomly arranged carbon atoms in case one of the first model. The electric current density ($\vec{J}$) can be

determined using Ohm's law: $\vec{J} = -\sigma \cdot \nabla\varphi$. Due to the poor electrical conductivity of AC, the charge mainly accumulates on the surface of AC. Under the effect of electric field, AC transforms into graphene sheets, then causing the rotation of graphene sheets to align in the direction of the current. In the second model, a rectangular shape with a size of 1 × 20 nm² represent the graphene sheet. There is an angle θ between the graphene and the current direction. θ was set between 10 and 90 degrees. The changes in electric free energy of the graphene sheets were studied at an applied voltage of 40 V, 80 V, 120 V, and 160 V. To investigate the changes in interlayer spacing of graphene sheets under the influence of an electric field, a third model was established. In this model, there are a total of 15 layers of graphene sheets, with each graphene layer represented by a rectangular shape measuring 1 × 20 nm². The changes in electric free energy were calculated during the variation in interlayer spacing of the graphene layers under voltages of 40 V, 80 V, 120 V, and 160 V. Considering the experimental results, the maximum interlayer spacing measured was 0.346 nm, while the minimum was 0.338 nm. Therefore, we only considered the changes in electric potential energy for 15 layers of graphene within a thickness range of 5.20 nm to 5.05 nm.

Acknowledgements The funding of the research was provided by the Air Force Office of Scientific Research (FA9550-22-1-0526), the Department of Energy, NETL (DE-FE0031794, J.M.T.) and the U.S. Army Corps of Engineers, ERDC (W912HZ-21-2-0050, J.M.T. and Y.Z.). The characterization equipment used in this project is partly from the Shared Equipment Authority (SEA) at Rice University.

Supporting Information. Additional spectra, graphs, images, and data (PDF).

Disclosures—Conflict of Interest

Rice University owns intellectual property on the flash Joule heating strategy. J. M. T. is a stockholder in Universal Matter Ltd., a company that has licensed the intellectual property from Rice University. J. M. T. is not an officer, director or employee of Universal Matter Ltd. All conflicts of interest are managed through regular disclosure to the Rice University Office of Sponsored Programs and Research Compliance.

References

1. Huang, P.; Zhu, R.; Zhang, X.; Zhang, W., Effect of Free Radicals and Electric Field on Preparation of Coal Pitch-Derived Graphene Using Flash Joule Heating. *J. Chem. Eng.* **2022,** *450,* 137999.

2. Wang, J.; Park, J.-H.; Lu, A.-Y.; Kong, J., Electrical Control of Chemical Vapor Deposition of Graphene. *J. Am. Chem. Soc.* **2022,** *144,* 22925-22932.

3. Xu, S.; Wang, S.; Chen, Z.; Sun, Y.; Gao, Z.; Zhang, H.; Zhang, J., Electric-Field-Assisted Growth of Vertical Graphene Arrays and the Application in Thermal Interface Materials. *Adv. Funct. Mater.* **2020,** *30,* 2003302.

4. Wan, M.; Yue, H.; Notarangelo, J.; Liu, H.; Che, F., Deep Learning-Assisted Investigation of Electric Field–Dipole Effects on Catalytic Ammonia Synthesis. *JACS Au* **2022,** *2,* 1338-1349.

5. Jesus, L. M.; Silva, R. S.; Raj, R.; M'Peko, J.-C., Electric Field-Assisted Ultrafast Synthesis of Nanopowders: A Novel and Cost-Efficient Approach. *RSC Adv.* **2016,** *6,* 107208-107213.

6. Morris, P. D.; McPherson, I. J.; Edwards, M. A.; Kashtiban, R. J.; Walton, R. I.; Unwin, P. R., Electric Field-Controlled Synthesis and Characterisation of Single Metal–Organic-Framework (Mof) Nanoparticles. *Angew. Chem. Int. Ed.* **2020,** *59,* 19696-19701.

7. Qin, R., Electric-Field-Induced Alignment of Electrically Neutral Disk-Like Particles: Modelling and Calculation. *Sci. Rep.* **2017,** *7,* 8449.

8. Palyanov, Y. N.; Borzdov, Y. M.; Sokol, A. G.; Bataleva, Y. V.; Kupriyanov, I. N.; Reutsky, V. N.; Wiedenbeck, M.; Sobolev, N. V., Diamond Formation in an Electric Field under Deep Earth Conditions. *Sci. Adv.* **2021,** *7,* eabb4644.

9. Zhang, X.; Qin, R., Electric Current-Driven Migration of Electrically Neutral Particles in Liquids. *Appl. Phys. Lett.* **2014,** *104,* 114106.

10. Luong, D. X.; Bets, K. V.; Algozeeb, W. A.; Stanford, M. G.; Kittrell, C.; Chen, W.; Salvatierra, R. V.; Ren, M.; McHugh, E. A.; Advincula, P. A.; Wang, Z.; Bhatt, M.; Guo, H.; Mancevski, V.; Shahsavari, R.; Yakobson, B. I.; Tour, J. M., Gram-Scale Bottom-up Flash Graphene Synthesis. *Nature* **2020,** *577,* 647-651.

11. Stanford, M. G.; Bets, K. V.; Luong, D. X.; Advincula, P. A.; Chen, W.; Li, J. T.; Wang, Z.; McHugh, E. A.; Algozeeb, W. A.; Yakobson, B. I.; Tour, J. M., Flash Graphene Morphologies. *ACS Nano* **2020,** *14,* 13691-13699.

12. Wyss, K. M.; Beckham, J. L.; Chen, W.; Luong, D. X.; Hundi, P.; Raghuraman, S.; Shahsavari, R.; Tour, J. M., Converting Plastic Waste Pyrolysis Ash into Flash Graphene. *Carbon* **2021,** *174,* 430-438.

13. Chen, W.; Ge, C.; Li, J. T.; Beckham, J. L.; Yuan, Z.; Wyss, K. M.; Advincula, P. A.; Eddy, L.; Kittrell, C.; Chen, J.; Luong, D. X.; Carter, R. A.; Tour, J. M., Heteroatom-Doped Flash Graphene. *ACS Nano* **2022,** *16,* 6646-6656.

14. Advincula, P. A.; Meng, W.; Eddy, L. J.; Beckham, J. L.; Siqueira, I. R.; Luong, D. X.; Chen, W.; Pasquali, M.; Nagarajaiah, S.; Tour, J. M., Ultra-High Loading of Coal-Derived Flash Graphene Additives in Epoxy Composites. *Macromol. Mater. Eng.* **2023,** *308,* 2200640.

15. Eddy, L. J.; Luong, D. X.; Beckham, J. L.; Wyss, K. M.; Cooksey, T.; Scotland, P.; Choi, C. H.; Chen, W.; Advincula, P.; Zhang, Z.; Macevski, V.; Tour, J., Automated Laboratory Kilogram-Scale Graphene Production from Coal. *Small Methods* **2023**.

16. Sattari, K.; Eddy, L.; Beckham, J. L.; Wyss, K. M.; Byfield, R.; Qian, L.; Tour, J. M.; Lin, J., A Scientific Machine Learning Framework to Understand Flash Graphene Synthesis. *Digit. Discov.* **2023,** *2,* 1209-1218.

17. Chen, W.; Wang, Z.; Bets, K. V.; Luong, D. X.; Ren, M.; Stanford, M. G.; McHugh, E. A.; Algozeeb, W. A.; Guo, H.; Gao, G.; Deng, B.; Chen, J.; Li, J. T.; Carsten, W. T.; Yakobson, B. I.; Tour, J. M., Millisecond Conversion of Metastable 2d Materials by Flash Joule Heating. *ACS Nano* **2021,** *15,* 1282-1290.

18. Wang, C.; Ping, W.; Bai, Q.; Cui, H.; Hensleigh, R.; Wang, R.; Brozena, A. H.; Xu, Z.; Dai, J.; Pei, Y.; Zheng, C.; Pastel, G.; Gao, J.; Wang, X.; Wang, H.; Zhao, J.-C.; Yang, B.; Zheng, X.; Luo, J.; Mo, Y.; Dunn, B.; Hu, L., A General Method to Synthesize and Sinter Bulk Ceramics in Seconds. *Science* **2020,** *368,* 521-526.

19. Chen, G.; Wang, Y.; Wang, X.; Zhao, Y.; Dong, Q.; Hao, L.; Hong, M.; Guo, M.; Qiao, H.; Xiong, W.; Hu, L., Target-Sintering of Single-Phase Bulk Intermetallics Via a Fast-Heating-Induced Rapid Interdiffusion Mechanism. *ACS Mater. Lett.* **2022,** *4,* 480-486.

20. Dong, Q.; Hong, M.; Gao, J.; Li, T.; Cui, M.; Li, S.; Qiao, H.; Brozena, A. H.; Yao, Y.; Wang, X.; Chen, G.; Luo, J.; Hu, L., Rapid Synthesis of High-Entropy Oxide Microparticles. *Small* **2022,** *18,* 2104761.

21. Chen, W.; Li, J. T.; Ge, C.; Yuan, Z.; Algozeeb, W. A.; Advincula, P. A.; Gao, G.; Chen, J.; Ling, K.; Choi, C. H.; McHugh, E. A.; Wyss, K. M.; Luong, D. X.; Wang, Z.; Han, Y.; Tour, J.

M., Turbostratic Boron–Carbon–Nitrogen and Boron Nitride by Flash Joule Heating. *Adv. Mater.* **2022,** *34,* 2202666.

22. Deng, B.; Carter, R. A.; Cheng, Y.; Liu, Y.; Eddy, L.; Wyss, K. M.; Ucak-Astarlioglu, M. G.; Luong, D. X.; Gao, X.; JeBailey, K.; Kittrell, C.; Xu, S.; Jana, D.; Torres, M. A.; Braam, J.; Tour, J. M., High-Temperature Electrothermal Remediation of Multi-Pollutants in Soil. *Nat. Commun.* **2023,** *14,* 6371.

23. Chen, W.; Salvatierra, R. V.; Li, J. T.; Kittrell, C.; Beckham, J. L.; Wyss, K. M.; La, N.; Savas, P. E.; Ge, C.; Advincula, P. A.; Scotland, P.; Eddy, L.; Deng, B.; Yuan, Z.; Tour, J. M., Flash Recycling of Graphite Anodes. *Adv. Mater.* **2023,** *35,* 2207303.

24. Deng, B.; Luong, D. X.; Wang, Z.; Kittrell, C.; McHugh, E. A.; Tour, J. M., Urban Mining by Flash Joule Heating. *Nat. Commun.* **2021,** *12,* 5794.

25. Deng, B.; Meng, W.; Advincula, P. A.; Eddy, L.; Ucak-Astarlioglu, M. G.; Wyss, K. M.; Chen, W.; Carter, R. A.; Li, G.; Cheng, Y.; Nagarajaiah, S.; Tour, J. M., Heavy Metal Removal from Coal Fly Ash for Low Carbon Footprint Cement. *Comms. Eng.* **2023,** *2,* 13.

26. Chen, W.; Chen, J.; Bets, K. V.; Salvatierra, R. V.; Wyss, K. M.; Gao, G.; Choi, C. H.; Deng, B.; Wang, X.; Li, J. T.; Kittrell, C.; La, N.; Eddy, L.; Scotland, P.; Cheng, Y.; Xu, S.; Li, B.; Tomson, M. B.; Han, Y.; Yakobson, B. I.; Tour, J. M., Battery Metal Recycling by Flash Joule Heating. *Sci. Adv.* **2023,** *9,* eadh5131.

27. Pimenta, M. A.; Dresselhaus, G.; Dresselhaus, M. S.; Cançado, L. G.; Jorio, A.; Saito, R., Studying Disorder in Graphite-Based Systems by Raman Spectroscopy. *Physical Chemistry Chemical Physics* **2007,** *9,* 1276-1290.

28. Dresselhaus, M. S.; Jorio, A.; Souza Filho, A. G.; Saito, R., Defect Characterization in Graphene and Carbon Nanotubes Using Raman Spectroscopy. *Philos. Trans. R. Soc., A* **2010,** *368,* 5355-5377.

29. Beckham, J. L.; Wyss, K. M.; Xie, Y.; McHugh, E. A.; Li, J. T.; Advincula, P. A.; Chen, W.; Lin, J.; Tour, J. M., Machine Learning Guided Synthesis of Flash Graphene. *Adv. Mater.* **2022,** *34,* 2106506.

30. Dudarev, S. L.; Botton, G. A.; Savrasov, S. Y.; Humphreys, C. J.; Sutton, A. P., Electron-Energy-Loss Spectra and the Structural Stability of Nickel Oxide: An LSDA+U Study. *Phys. Rev. B.* **1998,** *57,* 1505-1509.

31. Blöchl, P. E., Projector Augmented-Wave Method. *Phys. Rev. B.* **1994,** *50,* 17953-17979.

32. Perdew, J. P.; Burke, K.; Ernzerhof, M., Generalized Gradient Approximation Made Simple. *Phys. Rev. Lett.* **1996,** *77,* 3865-3868.

33. Monkhorst, H. J.; Pack, J. D., Special Points for Brillouin-Zone Integrations. *Phys. Rev. B.* **1976,** *13,* 5188-5192.

34. Grimme, S.; Antony, J.; Ehrlich, S.; Krieg, H., A Consistent and Accurate *Ab Initio* Parametrization of Density Functional Dispersion Correction (DFT-D) for the 94 Elements H-Pu. *J. Chem. Phys.* **2010,** *132,* 154104.

35. Zhao, Y.; Yakobson, B. I.; Smalley, R. E., Dynamic Topology of Fullerene Coalescence. *Phys. Rev. Lett.* **2002,** *88,* 185501.

36. Zhao, Y.; Lin, Y.; Yakobson, B. I., Fullerene Shape Transformations *Via* Stone-Wales Bond Rotations. *Phys. Rev. B.* **2003,** *68,* 233403.

37. Samsonidze, G. G.; Samsonidze, G. G.; Yakobson, B. I., Kinetic Theory of Symmetry-Dependent Strength in Carbon Nanotubes. *Phys. Rev. Lett.* **2002,** *88,* 065501.

TOC Graphic